Dispersed Voltage Control in Microgrids

Giovanni Massa, *Member, IEEE*, George Gross, *Fellow, IEEE*, Vincenzo Galdi, *Member, IEEE*, and Antonio Piccolo, *Member, IEEE*

***Abstract*—The deeper penetration of distributed energy resources (*DER*s) in microgrids (μgs) has led to their wider deployment in specific applications. The inherent variability in loads and in renewable energy resource outputs necessitates the development and implementation of effective voltage control strategies so as to reliably serve the loads, particularly under islanded operations mode. We propose a dispersed control strategy to maintain voltage levels within the operational limits by means of the *DER*s reactive and active power outputs. We implement an optimization approach and demonstrate the effectiveness and the robustness of the proposed voltage control scheme using a set of representative studies from the extensive testing of the simulation approach performed with the methodology. Simulation results demonstrate the absence of any opportunity cost to implement the control action and the maximization of active power production by renewable energy resources.**

***Index Terms*—Deepening penetration of variable energy resources, distributed energy resource variability, distributed voltage control, microgrid, reactive power support.**

Abbreviations

BESS	Battery Storage System
BMS	Battery Management System
CHP	Combined Heat and Power
DER	Distributed Energy Resource
DG	Distributed Generator
DN	Distribution Network
DR	Demand Response
DRR	Demand Response Resource
ESS	Energy Storage System
FC	Fuel Cell
g.c.m.	Grid Connected Mode
i.o.m.	Islanded Operations Mode
LLD	Lower Limit Deadband
LMP	Locational Marginal Price
μg	Microgrid
μT	Microturbine
NHV	Net Heat Value
PCC	Point of Common Coupling
PEI	Power Electronic Interface
PV	PhotoVoltaic
RE	Reactive Energy
s.o.c.	State of Charge
ULD	Upper Limit Deadband

Manuscript received May 14, 2015; revised September 09, 2015; accepted November 15, 2015. Date of publication December 09, 2015; date of current version August 17, 2016. Paper no. TPWRS-00673-2015.

G. Massa, V. Galdi, and A. Piccolo are with the Department of Industrial Engineering, University of Salerno, 84084 Fisciano (SA), Italy (e-mail: gmassa@unisa.it; vgaldi@unisa.it; apiccolo@unisa.it).

G. Gross is with the Department of Electrical and Computer Engineering, University of Illinois at Urbana-Champaign, Urbana, IL 61801 USA (e-mail: gross@illinois.edu).

Color versions of one or more of the figures in this paper are available online at http://ieeexplore.ieee.org.

Digital Object Identifier 10.1109/TPWRS.2015.2503393

I. Introduction

THE deepening penetration of distributed energy resources (*DER*s) has pointed out the need of new models capable to better represent the variability in the loads as well as the intrinsic variable and intermittent nature of such resources. Indeed, the *DER*s connected at the distribution level represent a complication in distribution network (*DN*) operations and control. On the other hand, the rapid deployment of smart grid technologies provides the opportunity to develop new techniques for the operations and control of *DN*s with integrated *DER*s under normal and contingency conditions [1]. In particular, the microgrid (μg) concept implementation provides a promising approach to optimally manage *DN*s with deep penetration of integrated *DER*s.

The different definitions, as well as the regulatory policy structure of a μg are discussed at length in [2]. In our work, we use the definition for μg as a group of interconnected *DER*s, including generators, storage devices and controllable loads, which, together with imports, can meet the internal demand and the contracted exports, working either in the connected or islanded operations mode with respect to the main grid. Due to their deeper penetration in *DN*s, *DER*s must be able to provide the various services required for secure μg operations: the generation-demand balance along all time-scales of interest and the provision of appropriate voltage control and reactive power support [3]. This paper focuses on the latter problem and presents an effective approach for voltage control issues that particularly addresses the local nature of reactive power.

The past voltage control work has focused on two main approach categories, centralized control strategies [4]–[6] and distributed or decentralized techniques [7]–[17]. In the latter category, schemes use various resources, including distributed generators (*DG*s), energy storage systems (*ESS*s) or demand response resources (*DRR*s). A proportional-integral controller based technique for voltage control in *DN*s using *DER*s is presented in [7]. The impact on voltage levels of photovoltaic (*PV*) generation and traditional control devices (such as *DN*s tap changers) is analyzed by [8] and [9]. The capability of

PV/Wind generators to provide voltage/reactive power control [10], [11] and to adjust their reactive and active power output [12] are respectively proposed for medium and low voltage *DN*s, while the storage of the excess energy in battery based *ESS*s (*BESS*s) is investigated in [13]. A voltage control strategy for weak *DN*s based on power electronic interfaces (*PEI*s) of *DG*s is proposed in [14]. An adaptive control system containing a neuro-fuzzy controller [15] and the utilization of *PV* systems and *BESS*s [16] to control voltage and frequency are proposed for grid connected and standalone μgs, respectively. Control approaches based on reactive power support [17] and a combination of voltage-droop control and a demand dispatch concept [18] are presented for islanded μgs.

Earlier approaches prove how the utilization of *DER*s could face the voltage control problem to guarantee a wider flexibility compared to traditional control strategies. The main lack of such approaches is that they focus on the utilization of only some of the *DER*s available within a μg to implement the voltage control actions and are usually applied to a single operations condition, looking at the grid-connected mode (*g.c.m.*) [8]–[15], or at the standalone/islanded operations mode (*i.o.m.*) [16], [17]. Furthermore, previous approaches do not include the voltage control schemes within a framework capable to guarantee a cost effective solution.

Within our work, we present a comprehensive utilization of the μg resources to meet voltage control needs, modeling the control capability of *DG*s, such as *PV*, wind and combined heat and power systems (*CHP*), *ESS*s, and *DRR*s. We explicitly address the voltage control issue through the formulation of dispersed voltage control strategies using *DER*s, in both the *g.c.m.* and the *i.o.m.* We perform the voltage control at the point of common coupling (*PCC*) between the *DER* and the μg feeder. We include in the strategy the constraints necessary to maintain the voltage within the specified limits through the appropriate deployment of reactive power support by *DER*s and/or active power production reduction if it becomes necessary. The control action specification provided by *DER*s is obtained from an optimization formulation that incorporates all the physical and regulatory constraints, including the *DER* capability curves, regulatory requirements, the power factor specifications, the network consideration in a market environment. Under *g.c.m.*, the demand is met with the imports from the main grid, with cost minimization as the appropriate objective function. Under the *i.o.m.*, the optimization is based on the incurred *DER* production costs to meet at least the critical load requirements. Whenever the *DER* capacities are inadequate to satisfy the loads, *DRR*s are deployed to ensure the critical loads are met. We illustrate the application of the proposed methodology with a set of representative studies from the extensive testing of the simulation approach we performed .

Simulation results show the effectiveness of the proposed approach to: a) utilize a unified strategy for the control of *DER*s connected to the μg feeder by means of *PEI*s; b) implement dispersed voltage control actions avoiding, as much as possible, the reduction of active power production from *DER*s; c) avoid the entailment of opportunity costs for the required control action; d) overcome the use of Volt/VAr devices that may face several challenges due to their interaction with *DER*s [19] and may be inadequate to furnish the required functionalities during the *i.o.m.*; e) guarantee critical loads served during the islanding condition. Furthermore, the proposed approach presents a cost effective solution that guarantees an economic operation for both the *g.c.m.* and the *i.o.m.*

TABLE I
*DER*s P AND Q CONTROL CAPABILITIES

***DER* type**	***DER* interface**	***p***	***q***
fixed-speed wind turbines	induction generator		-
small hydro reciprocating engines	synchronous generator		
variable-speed wind turbines		+	
PV			
fuel cell (*FC*)			
microturbine (μT)	*PEI*		$\pm$
flywheel			
battery storage systems (*BESS*)		$\pm$	
supercapacitor			
DRR	controlled switch	-	

The paper has five additional sections. In Section II, we address the basic concepts of the proposed μg's resources and control capabilities. In Section III, we introduce the proposed voltage control approach. We illustrate in Section IV the snapshot optimization approach for both the *g.c.m.* and the *i.o.m.* In Section V, we provide representative results from the extensive set of simulations performed on the μg system under study. We present concluding remarks in Section VI.

II. MICROGRID RESOURCES AND CONTROL CAPABILITIES

The conventional devices used to control voltage levels and to furnish reactive power support in *DN*s include fixed or switched capacitor banks, step voltage regulators and on-load tap-changing transformers. We make explicit use of *DER*s reactive and, in specific cases, active power outputs in the proposed voltage control scheme. We define the resources and their control capabilities as depicted in Table I. Within the table, symbols "+", "−", "±" describe the capability of the *DER* to act on the generated, absorbed, or both active and reactive power, respectively. We consider a general model in which the μg is equipped with the *DER*s described in the following.

*DG*s, such as *PV*, *Wind* and *CHP* plants are often connected to the grid by means of *PEI*s. These interfaces allow the *DG* to manage active/reactive power within the limits defined by the *PEI*s capability curves and the *DG* actual power limits, as outlined in [14].

*ESS*s, such as batteries, present active and reactive power control capabilities similar to *DG*s, thanks to *PEI*s. We model *ESS*s as limited energy plants, which must accomplish a full cycle over the study period. Taking into account the charge-discharge cycle efficiency η_s, given by the product between the *ESS* charging efficiency η_c and the discharging efficiency η_d, we obtain the following formulation:

$$\eta_c \varepsilon_c = \frac{\varepsilon_d}{\eta_d} \Rightarrow \eta_c \eta_d \varepsilon_c = \varepsilon_d \Rightarrow \eta_s \varepsilon_c = \varepsilon_d \tag{1}$$

where ε_c is the energy taken during the charge phase and ε_d the energy delivered to the load. Furthermore, we try to use the *ESS*

economically, assuring that the marginal cost of energy used to charge the storage system is less than the marginal cost displaced by the *ESS* discharge [20].

We take into account the potential impact of *DRR*s on voltage levels by means of variation of the active power absorbed by controllable loads. We integrate *DRR*s in the proposed voltage control approach taking into account the chronological limitations of typical demand response (*DR*) programs, considering these resources as a lowest effectiveness variable to use for the voltage control problem, in order to reduce the impact on customers.

III. Sensitivity Factors Based Local Voltage Control

We develop a voltage control methodology based on the sensitivity of voltage levels at the μg buses to active and reactive power variations from *DER*s. We consider a μg with $N+1$ buses and L lines. Thus, the set of buses is defined as $\mathcal{N} = \{n : n = 0, 1, 2, \ldots, N\}$, with bus 1 being the connection bus between the μg and the external main grid tie-line reference bus 0—for either a *DN* or a transmission network, depending on the size and location of the μg. We consider the M *PV* buses with $M < N$ to be numbered from 1 to M, and buses $M+1$ to N constituting the $N - M$ *PQ* buses. The amount M of *PV* buses can change depending on the μg configuration and the dispatched resources. We denote the index set of the *DG*s and *DRR*s as $\mathcal{S} = \{s_i : i = 1, 2, \ldots, S\}$ and $\mathcal{R} = \{r_j : j = 1, 2, \ldots, R\}$.

We use the resources in $\mathcal{S} \cup \mathcal{R}$ to control the network voltages. We assume that it is possible to connect a single μg bus $n \in \mathcal{N}$ to multiple resources of $\mathcal{S} \cup \mathcal{R}$. Thus, we define such a mapping function f capable to implement the resource mapping in order to associate each resource in $\mathcal{S} \cup \mathcal{R}$ to the corresponding connection node $n \in \mathcal{N}$. We define the mapping f as $\mathcal{S} \mapsto \mathcal{N} : s_i \in \mathcal{S} \to n \in \mathcal{N}$ and $\mathcal{R} \mapsto \mathcal{N} : r_j \in \mathcal{R} \to n \in \mathcal{N}$. We denote by $\mathcal{L} = \{l : l = 1, 2, \ldots, L\}$ the set of lines that connect the buses in $\mathcal{N}$ and associate with each line $l \in \mathcal{L}$ the node pair (n, h) so that $l \leftrightarrow (n, h)$. We define the analysis period set as $\mathcal{T} = \{t_k : k = 1, 2, \ldots, K\}$ and we denote the voltage amplitudes and angles for a given time step $t_k \in \mathcal{T}$ as the following vectors:

$$\begin{aligned} \boldsymbol{v}[t_k] &\triangleq [v_1[t_k], v_2[t_k], \ldots, v_N[t_k]]^T \\ \boldsymbol{\vartheta}[t_k] &\triangleq [\vartheta_1[t_k], \vartheta_2[t_k], \ldots, \vartheta_N[t_k]]^T . \end{aligned} \tag{2}$$

Being bus 0 associated to the external grid, the real effects of the μg components actions on the reference bus are taken into account by modeling bus 1, that represents the connection bus between the μg and the external grid. We define the voltage control problem as the constraint to maintain the voltage profile $v_n[t_k]$ at each bus $n \in \mathcal{N}$ as dictated by operational policy or regulatory requirements for each time snapshot t_k:

$$v_n^m \le v_n[t_k] \le v_n^M \quad \forall n \in \mathcal{N}, \forall t_k \in \mathcal{T}. \tag{3}$$

We denote the net active and reactive power injection at each node $n \in \mathcal{N}$ by $p_n[t_k]$ and $q_n[t_k]$. Thus, we define:

$$\begin{aligned} \boldsymbol{p}[t_k] &\triangleq [p_1[t_k], p_2[t_k], \ldots, p_N[t_k]]^T \\ \boldsymbol{q}[t_k] &\triangleq [q_1[t_k], q_2[t_k], \ldots, q_N[t_k]]^T . \end{aligned} \tag{4}$$

We take into account the constraints coming from the power flow equations. If g_{nh} and b_{nh} represent the elements of the μg conductance and susceptance matrices, respectively, we obtain:

$$\begin{aligned} p_n[t_k] &= \sum_{h \in \mathcal{N}} v_n[t_k] v_h[t_k] \left(g_{nh} \cos \vartheta_{nh}[t_k] + b_{nh} \sin \vartheta_{nh}[t_k]\right) \\ q_n[t_k] &= \sum_{h \in \mathcal{N}} v_n[t_k] v_h[t_k] \left(g_{nh} \sin \vartheta_{nh}[t_k] + b_{nh} \cos \vartheta_{nh}[t_k]\right) \end{aligned} \tag{5}$$

where $\vartheta_{nh}[t_k] = \vartheta_n[t_k] - \vartheta_h[t_k]$ represents the phase angle between $v_n[t_k]$ and $v_h[t_k]$.

Due to the time step t_k, that defines the resolution of the snapshot analysis, we assume the voltage ($\Delta v_n[t_k]$) and angle ($\Delta \vartheta_n[t_k]$) variations occurring during the time interval $[t_{k-1}, t_k]$, represented by a total variation occurring at the snapshot instant t_k. Thus, voltage and angle are delineated by constant values between t_{k-1} and t_k. We compute the variation in voltage magnitude and angle during two consecutive time steps respectively as $\Delta v_n[t_k] = v_n[t_k] - v_n[t_{k-1}]$ and $\Delta \vartheta_n[t_k] = \vartheta_n[t_k] - \vartheta_n[t_{k-1}]$. These variations will be related to variation of active and/or reactive power $\Delta p_n[t_k]$ and $\Delta q_n[t_k]$ by the following relationship (6), representing the linearization of the power flow equations around the operating point at a given instant. Each element $\boldsymbol{J}_{xy}[t_k]$ represents the Jacobian submatrix obtained by the power flow equations linearization around the operation point connecting the Δx variation to the Δy effect:

$$\begin{bmatrix} \boldsymbol{J}_{p\vartheta}[t_k] & \boldsymbol{J}_{pv}[t_k] \\ \boldsymbol{J}_{q\vartheta}[t_k] & \boldsymbol{J}_{qv}[t_k] \end{bmatrix} \begin{bmatrix} \Delta \boldsymbol{\vartheta}[t_k] \\ \Delta \boldsymbol{v}[t_k] \end{bmatrix} = \begin{bmatrix} \Delta \boldsymbol{p}[t_k] \\ \Delta \boldsymbol{q}[t_k] \end{bmatrix} . \tag{6}$$

In transmission systems, the terms $\boldsymbol{J}_{pv}[t_k]$ and $\boldsymbol{J}_{q\vartheta}[t_k]$ are assumed negligible compared to $\boldsymbol{J}_{p\vartheta}[t_k]$ and $\boldsymbol{J}_{qv}[t_k]$ because of the high reactance over resistance ratio (X/R). This assumption allows an effective decoupling of the effects of active and reactive power variations on voltage magnitudes and angles. In *DN*s and μgs, this assumption cannot be made because of the lower X/R ratios of the lines [14]. Thus, to determine the effects of active and reactive power variations at the *PCC* on voltage levels, we consider (6).

Taking into account the *DER* control capabilities defined in Section II, the control algorithm operates only if the voltage at the *DER PCC* approaches the operational limits. We define two limit dead-bands as depicted in Fig. 1.

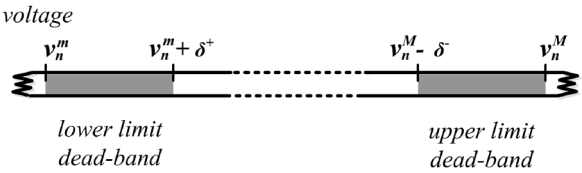

Fig. 1. The control dead-bands of voltage magnitude variable.

The dead-bands are respectively large δ^- and δ^+, meaning their distance from the maximum and minimum allowed voltage limit, respectively, and are placed before these limits.[1] If the voltage level at a generic bus n connected to such a resource reaches the dead-band level, such as the upper limit dead-band

[1]The dead-bands δ^- and δ^+ could be computed offline or by applying a procedure similar to the one described in [21].

(*ULD*), the controller acts as in the following, depending on the resource available at bus n. In this case, we define the desired voltage recovery amount, necessary to maintain voltage levels within operational limits, as:

$$\Delta v_n^*[t_k] = v_n[t_k] - \left(v_n^M - \delta^-\right). \tag{7}$$

Considering a general approach for a given operating point, we define $\Delta \boldsymbol{v}^*[t_k]$ and $\Delta \boldsymbol{\vartheta}^*[t_k]$ as the vectors representing the desired voltage and angle variations at the μg buses. We explicitly deploy the equality constraint to obtain the control action that uses the functional dependencies of the state variables:

$$\begin{bmatrix} \boldsymbol{J}_{p\vartheta}[t_k] & \boldsymbol{J}_{pv}[t_k] \\ \\ \boldsymbol{J}_{q\vartheta}[t_k] & \boldsymbol{J}_{qv}[t_k] \end{bmatrix} \begin{bmatrix} \Delta \boldsymbol{\vartheta}^*[t_k] \\ \\ \Delta \boldsymbol{v}^*[t_k] \end{bmatrix} = \begin{bmatrix} 0 \\ \\ \Delta \boldsymbol{q}[t_k] \end{bmatrix}. \tag{8}$$

From the triangularization of the matrix in (8) we obtain:

$$\boldsymbol{J}_q^{eq}[t_k] \Delta \boldsymbol{v}^*[t_k] = \Delta \boldsymbol{q}[t_k] \tag{9}$$

where:

$$\boldsymbol{J}_q^{eq}[t_k] = \boldsymbol{J}_{qv}[t_k] - \boldsymbol{J}_{q\vartheta}[t_k] \left(\boldsymbol{J}_{p\vartheta}[t_k]\right)^{-1} \boldsymbol{J}_{pv}[t_k] \tag{10}$$

and we implicitly assume that $\boldsymbol{J}_{p\vartheta}[t_k]$ is not singular.

We use the relation in (9) to determine the reactive power support shared among the *DER*s connected to the respective buses for which a voltage variation is required, taking into account the *DER* costs defined in next Section. If, for such a bus $n \in \mathscr{N}$, the required reactive power support is greater than the overall capability limits of the available controllable resources, an active power curtailment takes place for the resources connected to that bus.

The procedure concerning the lower limit dead-band (*LLD*) violation is almost symmetrical to the one illustrated for the *ULD* and it is not described here due to space limitation. The main difference is that in the *LLD* violation case we do not implement active power increase actions from renewables to boost the voltage level because they are dispatched at their maximum active power production. We outline further details concerning the proposed control methodology in Appendix A.

IV. Optimization Framework

We integrate the voltage control procedure into a snapshot based 24 hours optimization routine with computed steps every 10 minutes. The objective function of the optimization procedure is to minimize production costs within the μg. We assume that a single entity manages the μg, thus solving the optimization problem in order to maximize the total benefits to the μg participants—loads and resources—which under certain conditions may be equivalent to minimize the costs of the services provided. In order to maximize the environmental benefits from renewable energy resources, we manage these resources dispatching all their available power.

In the *g.c.m.*, we consider locational marginal prices (*LMP*s) from the day ahead market for the main reference bus prices. We integrate *DRR*s in the optimization strategy taking into account the chronological limitations of typical *DR* programs. We define a *modulation window* as the time window during which the optimization framework asks to such a *DRR* (or more than one) to furnish support to solve the voltage control problem (e.g. by reducing its power consumption during the time window). If such a *DRR* gives its contribution to the control action during the *modulation window*, the optimization framework computes the optimal time window for the *recovery action*, during which the *DRR* can recover the modulated energy (or only a portion of it, depending on the optimization framework constraints and the production costs) with a given maximum power peak profile. Thus, we define a subset of the analysis period set for the *modulation window* ($\mathscr{T}_c \subset \mathscr{T}$) and a different subset ($\mathscr{T}_r \subset \mathscr{T}$) for the *recovery action*. We assume the *DRR* to be not obliged to recover the modulated energy.

We define the objective function as in (11), where $c_0(p_0[t_k])$ is the *LMP* and $c_s(p_s[t_k])$ is the production cost of *DG*s and *ESS*s.

$$\min_{p_s} \sum_{t_k \in \mathscr{T}} \left(c_0\left(p_0[t_k]\right) + \sum_{s \in \mathscr{S}} c_s\left(p_s[t_k]\right) \right). \tag{11}$$

We take into account the constraints in (3), (5) and (12) to (22) $\forall s \in \mathscr{S}$, $\forall n \in \mathscr{N}$, $\forall t_k \in \mathscr{T}$ and $\forall l \in \mathscr{L}$:

(a) power factor:

$$\zeta^m \leq \zeta_s = \frac{p_s[t_k]}{\sqrt{p_s^2[t_k] + q_s^2[t_k]}} \leq 1.0 \tag{12}$$

(b) generator capability curves:

$$q_s^m[t_k] \leq q_s[t_k] \leq q_s^M[t_k] \tag{13}$$

$$p_s^m[t_k] \leq p_s[t_k] \leq p_s^M[t_k] \tag{14}$$

(c) generator ramping limits:

$$-\Delta p_s^m \leq \Delta p_s[t_k] \leq \Delta p_s^M \tag{15}$$

(d) line limits:

$$a_l[t_k] \leq a_l^M[t_k] \tag{16}$$

(e) *ESS*:

$$\varepsilon_s^m[t_k] \leq \varepsilon_s[t_k] \leq \varepsilon_s^M[t_k] \tag{17}$$

$$\Delta p_s^m[t_k] \leq \Delta p_s[t_k] \leq \Delta p_s^M[t_k] \tag{18}$$

$$0 \leq u^c[t_k] + u^d[t_k] \leq 1 \quad u^c[t_k], u^d[t_k] \in \{0,1\} \tag{19}$$

(f) *DRR*:

$$\sum_{\substack{r \in \mathscr{R} \\ t_k \in \mathscr{T}_c}} \Delta p_r[t_k] \Delta t_k \leq \sum_{\substack{r \in \mathscr{R} \\ t_k \in \mathscr{T}_r}} \rho_r p_r[t_k] \Delta t_k. \tag{20}$$

$$\sum_{\substack{r \in \mathscr{R} \\ t_k \in \mathscr{T}_c}} \Delta p_r[t_k] \Delta t_k \geq \sum_{\substack{r \in \mathscr{R} \\ t_k \in \mathscr{T}_r}} \Delta p_r[t_k] \Delta t_k \tag{21}$$

$$\sum_{\substack{r \in \mathscr{R} \\ t_k \in \mathscr{T}_c}} c_r\left(p_r[t_k]\right) \geq \sum_{\substack{r \in \mathscr{R} \\ t_k \in \mathscr{T}_r}} c_r\left(p_r[t_k]\right). \tag{22}$$

Constraint (12) is related to generators power factors requirements imposed by National and International Standards. Concerning (13) and (14), we represent the physical generation capabilities—hard constraints that cannot be violated explicitly

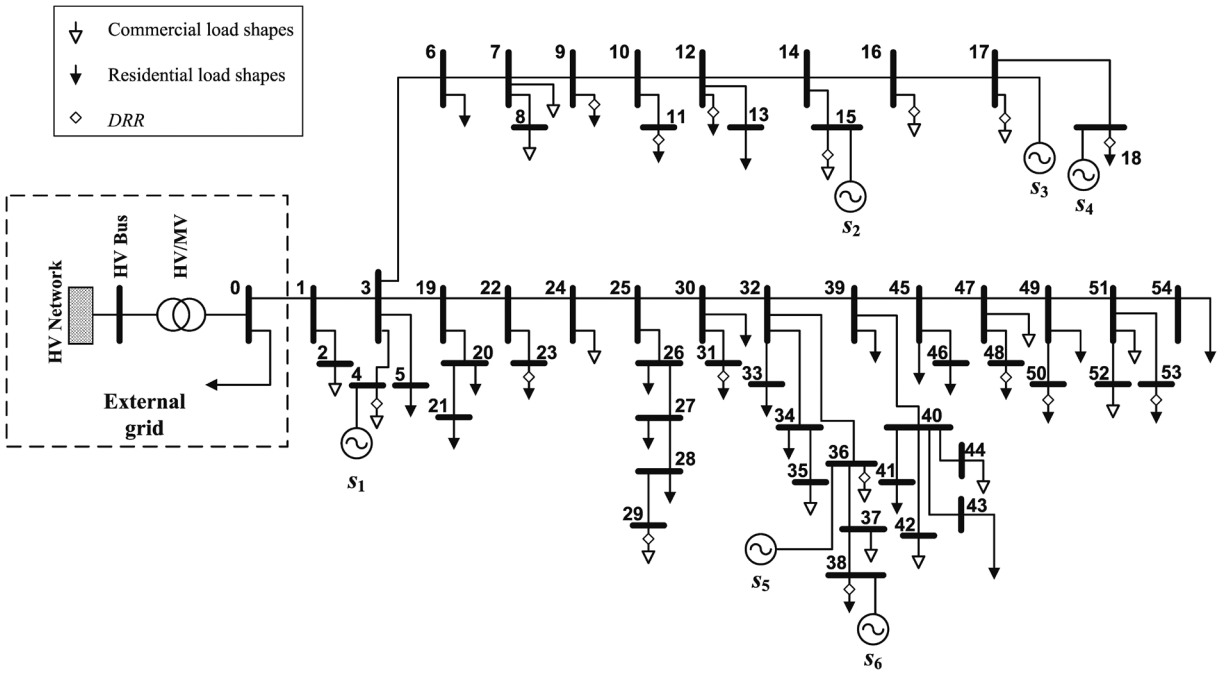

Fig. 2. The topology of the μg under study.

so as to account for their impacts on the determination of the controls that are deployed. We make use of the model outlined in Appendix A [14] for *DER*s connected by means of *PEI*s, such as *PV*s, *Wind*, *BESS*s and μTs. We take into account the ramping requirements related to generators in (15), while $a_l[t_k]$ in (16) represents the apparent power flowing through each line l, necessary to take into account thermal limits. *ESS* requirements account for storage capacity limits (17), charging/discharging rates (18) and charging/discharging status (19) during the analysis period, in order to obtain a general formulation. For *DRR*s, ρ_r represents the percentage of the *DRR* actual power available to *DR* (20), while $\Delta p_r[t_k]$ and $c_r(p_r[t_k])$ respectively represent the power variation (21) and the controllable load cost (22) during the *modulation window/recovery action*. Due to the general approach to the μg concept, in the *i.o.m.* it could be possible to size the μg in order to match only critical loads, meaning that the internal resources could not be capable to satisfy all the internal loads during the *i.o.m.* Thus, we consider the interval of the *DRR* participation to the resource mix to be dictated by the constraints related to the other generators in the μg (e.g. availability and ratings). The proposed approach allows the recovery of the curtailed energy only if there is such a time slot in which a generation surplus takes place and the *ESS*s within the network are at their maximum state of charge (*s.o.c.*). The following equilibrium constraint is added to the *i.o.m.* formulation:

$$\sum_{\substack{s\in\mathscr{S}\\ t_k\in\mathscr{T}}} p_s[t_k] + \sum_{\substack{r\in\mathscr{R}\\ t_k\in\mathscr{T}_C}} p_r[t_k] - \sum_{\substack{r\in\mathscr{R}\\ t_k\in\mathscr{T}_R}} p_r[t_k] = \sum_{\substack{d\in\mathscr{D}\\ t_k\in\mathscr{T}}} p_d[t_k] \quad (23)$$

where $\mathscr{D} = \{d : n = 0, 1, 2, \ldots, D\}$ represents the set of loads that do not participate to the *DR* control support. In the *i.o.m.*, we consider a particular case of (11), with the objective function finalized to minimize the production cost from the internal resources:

$$\min_{p_s} \sum_{t_k\in\mathscr{T}} \left(\sum_{s\in\mathscr{S}} c_s\left(p_s[t_k]\right) \right). \quad (24)$$

In the *i.o.m.*, we consider explicitly the constraints (3), (5) and (12) to (23).

The optimization framework introduced within this Section represents the basis for the control strategy developed in our approach.

V. Simulation Results

We provide a set of representative studies from the extensive testing of the simulation approach we performed to illustrate the functioning of the proposed dispersed control strategy.[2] We base our simulations on the modified test μg depicted in Fig. 2, representative of a typical medium voltage radial *DN*. We use the system in [22] and we modify the peak power of a few buses. We report the overall test μg data in Table II.

We remove the capacitor banks contained in the original reference network to show the *DER*s control capabilities related to the proposed approach. We integrate into the test network three *PV* systems, two μT *CHP* plants and an *ESS*, with their characteristics given in Table III.

We assume the *CHP* composed by fast commuting devices, characterized by slew-rate values capable to guarantee satisfying ramping rates, in order to assure the adaptation of the state changes within the simulation snapshot interval Δt_k. Furthermore, we consider that the *CHP* characteristics should be flexible enough to guarantee load-following performance, in order

[2]The simulation snapshot analysis runs on a 10 minutes time step base in order to assure the adaptation of the state changes [6], [11], [14]

TABLE II
μg NETWORK DATA

Network Data																	
Line Data				Line Data				Line Data				Load Data		Load Data		Load Data	
from	to	R [Ω]	X [Ω]	from	to	R [Ω]	X [Ω]	from	to	R [Ω]	X [Ω]	bus	[MVA]	bus	[MVA]	bus	[MVA]
0	1	0.160	0.388	3	19	0.138	0.334	36	37	0.610	0.238	2	0.057	27	0.038	47	0.296
1	2	0.824	0.315	19	20	0.251	0.096	37	38	2.349	0.964	4	0.121	28	0.044	48	0.045
1	3	0.144	0.349	20	21	1.818	0.695	32	39	0.115	0.278	5	0.049	29	0.053	49	0.145
3	4	1.026	0.421	19	22	0.225	0.542	39	40	0.159	0.384	6	0.053	30	0.223	50	0.058
3	5	0.741	0.466	22	23	0.127	0.028	40	41	0.934	0.383	7	0.047	31	0.123	51	0.047
3	6	0.528	0.468	22	24	0.284	0.687	40	42	0.506	0.163	8	0.068	33	0.094	52	0.131
6	7	0.358	0.314	24	25	0.171	0.414	40	43	0.095	0.195	9	0.048	34	0.097	53	0.261
7	8	2.032	0.798	25	26	0.414	0.386	40	44	1.915	0.769	11	0.094	35	0.281	54	0.315
7	9	0.502	0.441	26	27	0.210	0.196	39	45	0.157	0.379	12	0.067	36	0.117	Other Parameters	
9	10	0.372	0.327	27	28	0.395	0.369	45	46	1.641	0.670	13	0.057	37	0.131		
10	11	1.431	0.999	28	29	0.248	0.232	45	47	0.081	0.196	15	0.053	38	0.030		
10	12	0.429	0.377	25	30	0.205	0.495	47	48	1.727	0.709	16	0.057	39	0.130		
12	13	0.671	0.257	30	31	0.263	0.073	47	49	0.112	0.270	17	0.112	41	0.083	Vbase = 12 kV	
12	14	0.457	0.401	30	32	0.071	0.171	49	50	0.674	0.275	18	0.087	42	0.057	Sbase = 1 MVA	
14	15	1.008	0.385	32	33	0.625	0.273	49	51	0.070	0.170	21	0.063	43	0.121	Zbase = 144	
14	16	0.153	0.134	32	34	0.001	0.209	51	52	2.041	0.780	23	0.135	44	0.134		
16	17	0.971	0.722	34	35	2.018	0.829	51	53	0.813	0.334	24	0.100	45	0.234		
17	18	1.885	0.721	32	36	1.062	0.406	51	54	0.141	0.340	26	0.048	46	0.196		

TABLE III
*DER*S INTEGRATED INTO THE TEST SYSTEM

s	*type*	bus no.	*p* [MVW]
1	μT	4	1
2	*PV*	15	0.5
3	*PV*	17	1
4	*PV*	18	1.8
5	*ESS*	36	1
6	μT	38	1

TABLE IV
*DRR*S CONSIDERED WITHIN THE TEST SYSTEM

r	bus no.	*r*	bus no.
1	4	9	23
2	9	10	29
3	11	11	31
4	12	12	36
5	15	13	38
6	16	14	48
7	17	15	50
8	18	16	53

to facilitate the generation-demand balance, particularly relevant under the *i.o.m*. Thus, within our study, we choose modular μT systems, capable to offer services such as load following control with high-level efficiencies [23]. Each μT is composed by five systems (rated power 200 kVA each one) and a central controller capable to coordinate the single units in order to guarantee high-level efficiencies at partial load.

We consider each μT system to produce at least 200 kW power in the *g.c.m*. in order to produce heating and/or cooling energy for the μg heating district needs.[3] Concerning the μT production cost model, we take into account the simplified model outlined in (25), as in the following:

$$c_s\left(p_s[t_k]\right) = \sum_{t_k \in \mathscr{T}} \eta_s\left(p_s[t_k]\right) \xi \pi NHR\, p_s[t_k] \Delta t_k \qquad (25)$$

where $\eta_s(p_s[t_k])$ represents the efficiency curve of the μT system, ξ is the fuel cost $[\$/\mathrm{m}^3]$ and π is a conversion coefficient to estimate the energy contained within a certain amount of fuel $[\mathrm{MJ}/\mathrm{m}^3]$. NHR represents the net heat rate of the μT system. In our case, we consider $NHR = 11600$ kJ/kWh and the efficiency curve given by [23].

We adopt an *ESS* model based on real data available from commercial products. We consider a battery based *ESS* characterized by a 1 MW peak power rating and energy storage capacity of 3 MWh [24]. To complete the list of the available controllable resources, we show in Table IV the list of loads considered as *DRR*s.

We implement the simulation framework taking into account real *PV* power profiles for winter ($\mathscr{W}$) and summer ($\mathscr{Y}$). We represent here two days per season, a cloudy day and a sunny day, as in Fig. 3. We consider load shapes defined as typical residential and commercial customers weekday (*wd*) and weekend (*we*) patterns, as in Fig. 4 [25].

We show representative results for both the *g.c.m*. and the *i.o.m*. for the worst situation concerning voltage control, a $\mathscr{Y}$ sunny *we* day.

As Fig. 5 shows, a violation of voltage limits occur in both cases without an appropriate control strategy. For the *i.o.m*., the situation presents two violations, respectively on bus 17 and bus 18.

[3]We do not model the dynamics of the excess heating power produced by μTs because it is beyond the scope of the paper. We only mention, here, that excess power could be used for heating/cooling needs or thermal storage.

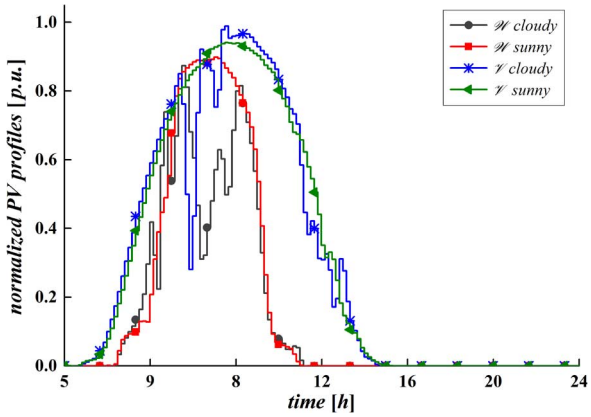

Fig. 3. Power output profile of each *PV* resource s_2, s_3 and s_4 for various day types.

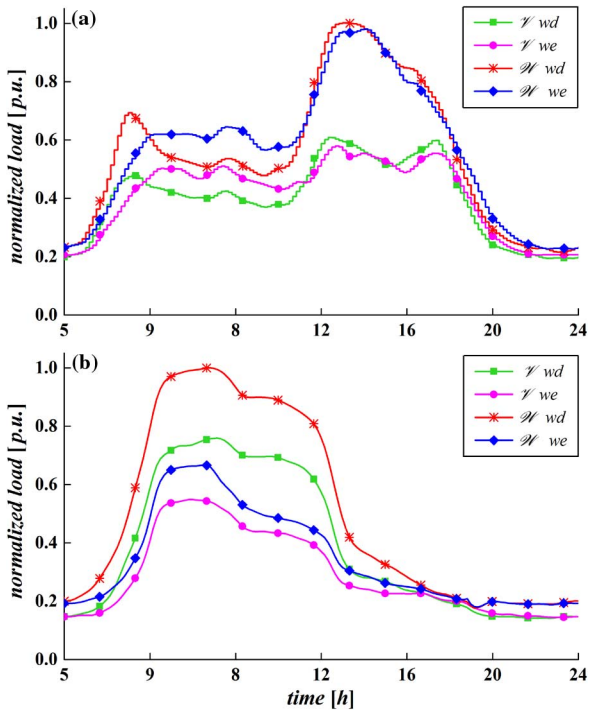

Fig. 4. Daily load shapes—(a) *g.c.m.*—(b) *i.o.m.*

We run the optimization algorithm containing the voltage control method to optimize the production costs for the *g.c.m.* and *i.o.m.*, obtaining the resource mix shown in Fig. 6. It is worth to note the different scheduling of s_1, s_5 and s_6, due to the absence, in the *i.o.m.*, of the main grid connection. The optimization approach reaches the objective of voltage control by means of the reactive power support profiles illustrated in Fig. 7. It is worth to note that in the *i.o.m.* both the generators connected to the buses affected by voltage rise give their contribution to the control action by means of reactive power support. Controlled voltage profiles for the interest buses are depicted in Fig. 8. Voltage is maintained within operational limits by local reactive power support and without any active power curtailment. Thus, no opportunity cost is involved by the proposed approach.

In the following tables, we give information concerning total costs and reactive power support obtained as part of the extensive tests we performed. We also introduce the parameter reactive energy (*RE*). Even if this parameter is not a real energy measurement unit, it gives the idea of the overall reactive power contribution over time during the 24 hours based snapshot simulation period. It is worth to note in Table V, concerning *g.c.m.* optimization, that the total operation cost in case of clouds is

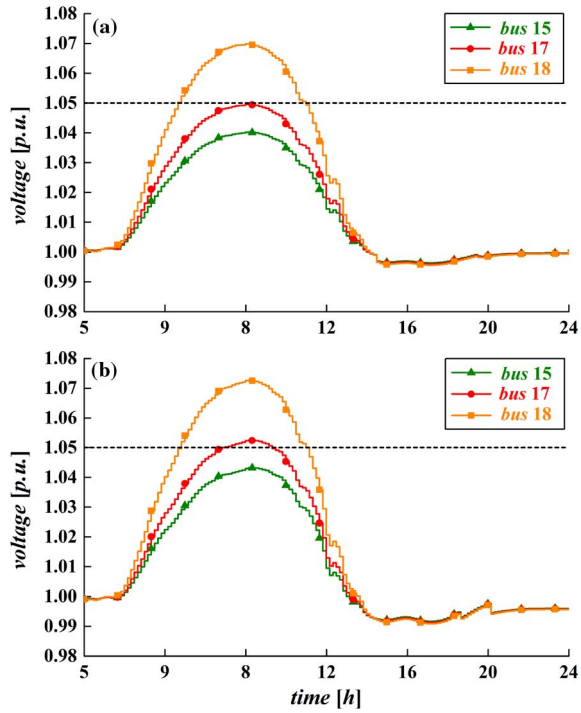

Fig. 5. Uncontrolled voltage profiles—(a) *g.c.m.*—(b) *i.o.m.*

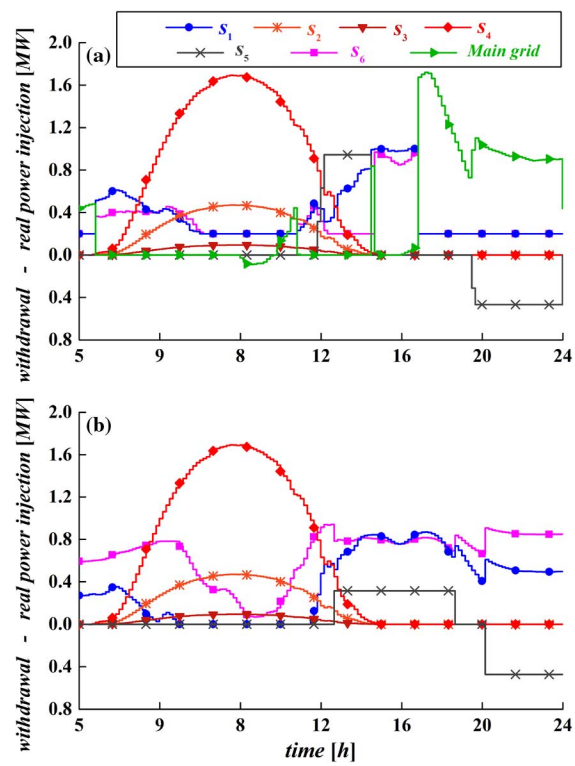

Fig. 6. Active power—(a) *g.c.m.*—(b) *i.o.m.*

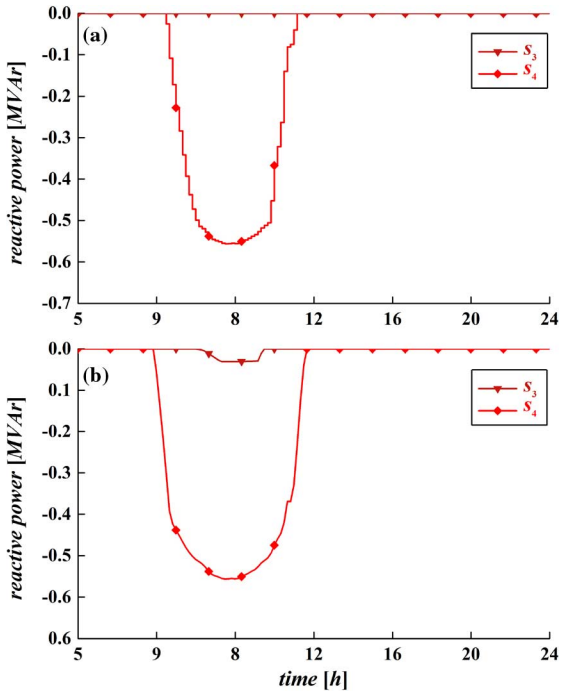

Fig. 7. Reactive power support—(a) *g.c.m.*—(b) *i.o.m.*

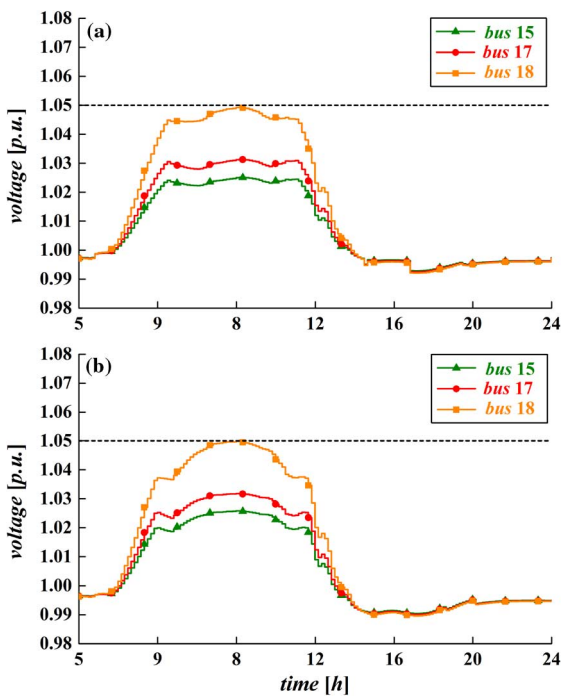

Fig. 8. Controlled voltage profiles—(a) *g.c.m.*—(b) *i.o.m.*

TABLE V
G.C.M. COSTS AND REACTIVE POWER SUPPORT

summer		total cost [k$]	total Q	total *RE*
cloudy	*wd*	6.28	15.88	5.29
	we	5.80	16.56	5.52
cloudy	*wd*	6.45	15.25	5.09
	we	5.99	15.81	5.27

higher than in the sunny case, because of the reduced contribution by *PV*s.

TABLE VI
I.O.M. COSTS AND REACTIVE POWER SUPPORT

summer		total cost [k$]	total Q	total *RE*
cloudy	*wd*	6.68	19.93	6.64
	we	5.88	20.92	6.98
cloudy	*wd*	6.78	18.86	6.29
	we	5.98	19.11	6.37

For the *i.o.m.*, in Table VI we show representative results concerning the same days as in the *g.c.m.* case. Results show a higher reactive power support contribution compared to the *g.c.m.*, mainly due to the absence of the main grid reference bus connection.

Concerning the *DRR*s, we know that *DRR*s are least effective in terms of providing voltage control and such a result is in line with the low sensitivity associated with such resources. Thus, we present the concept of *DRR* incrementing the load to implement a voltage reduction, as introduced in [18], as a least effective resource to use for the sensitivity factors based approach. From the extensive set of simulations we performed, we gained the confirmation of a small impact of this control component on the voltage profiles, confirming the necessity to consider it as a last resource to use.

VI. CONCLUSIONS

In this paper, we presented the development and testing of a dispersed voltage control technique for μg applications, capable to avoid voltage limits infringement at the *PCC* between the *DER* and the μg feeder. Compared to earlier approaches, we focused on a comprehensive utilization of the *DER*s available within the μg in order to implement the control actions, for both the *g.c.m.* and the *i.o.m.* We modeled *DER*s to be incorporated within an optimization framework taking into account all the physical and regulatory constraints. We run the optimization approach for both the *g.c.m.* and the *i.o.m.*, proving its cost effective characteristics.

Simulation results show the effectiveness of the proposed approach to implement an optimized scheduling of the μg resources while implementing the voltage control action without the entailment of any opportunity cost. Furthermore, it allows overcoming the utilization, at least in part, of traditional voltage control devices, such as on-load tap changers and capacitor banks.

APPENDIX A

We assume the Jacobian matrix defined in (6) to be non-singular, meaning the absence of voltage collapse. Indeed, for a given $\Delta q_n[t_k]$, the voltage stability region is defined by the region where $\Delta q_n[t_k]/\Delta v_n[t_k] > 0$. The critical point is represented by the point in which $\Delta q_n[t_k]/\Delta v_n[t_k] = 0$, followed by the unstable region in which $\Delta q_n[t_k]/\Delta v_n[t_k] < 0$. A similar approach can be used to define the $p_n[t_k]$ vs. $v_n[t_k]$ stability region. We suppose to work away from the critical operating point. Indeed, previous works on voltage stability have proved the increase of the voltage stability margins for deepening *DG* penetration [26]. Furthermore, the work in [27] proved that bounding

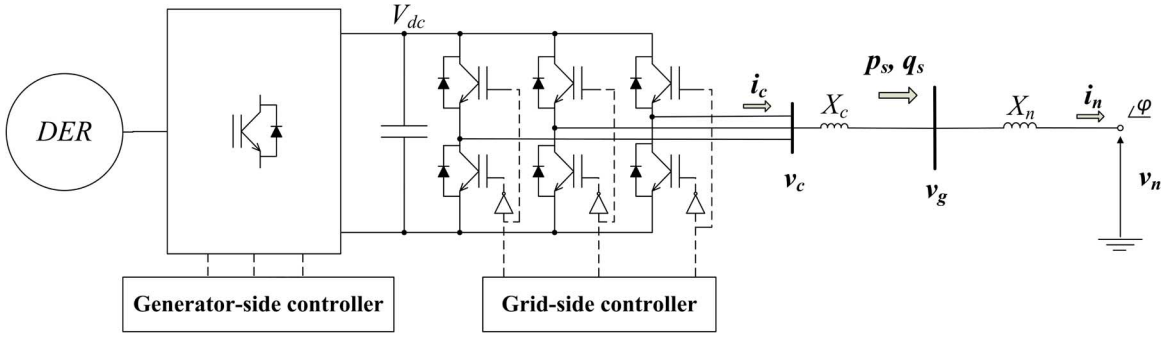

Fig. A.1. *PEI* schematic representation.

the control action under certain limits ensures the stability of computations around the operating point. In particular, we assume $\boldsymbol{J}_{p\vartheta}[t_k]$ and $\boldsymbol{J}_{q\vartheta}[t_k]$ to be non-singular for the given operating points. If the overall available reactive power support is less than required to guarantee an appropriate control action, we update the sensitivity factors for the new working point and compute an active power curtailment by (A.1), with $\boldsymbol{J}_p^{eq}[t_k]$ being (A.2):

$$\Delta \boldsymbol{p}^*[t_k] = \boldsymbol{J}_p^{eq}[t_k] \Delta \boldsymbol{v}^{**}[t_k] \tag{A.1}$$

where:

$$\boldsymbol{J}_p^{eq}[t_k] = \boldsymbol{J}_{pv}[t_k] - \boldsymbol{J}_{p\vartheta}[t_k] \left(\boldsymbol{J}_{q\vartheta}[t_k]\right)^{-1} \boldsymbol{J}_{qv}[t_k] \tag{A.2}$$

Concerning *PEI* based *DER*s (depicted in Fig. A.1), in the following we model the capability curve equations required for the control action. We start from the equations necessary to compute the generator active (p_s) and reactive (q_s) power for a *DER* connected to a *DN*:

$$\begin{aligned} p_s[t_k] &= v_n[t_k] i_n[t_k] \sin \phi_n[t_k] \\ q_s[t_k] &= \left(v_n[t_k] \sin \phi_n[t_k] + X_n i_n[t_k]\right) i_n[t_k] \end{aligned} \tag{A.3}$$

where $v_n[t_k]$, $i_n[t_k]$ and X_n represent the voltage, current and reactance at the *PCC*. Taking into account the root mean square of the converter voltage $v_n[t_k]$ and working on the equations, it is possible to obtain the first circular constraint due to the converter voltage $v_c[t_k]$, as stated by (A.4).

$$p_s^2[t_k] + \left(q_s[t_k] + \frac{v_s^2[t_k]}{X_c}\right)^2 \leq \left(\frac{v_c[t_k] v_s[t_k]}{X_c}\right)^2 \tag{A.4}$$

With an analogous approach, we state the circular constraint imposed by the converter current $i_c[t_k]$, taking into account the non-symmetrical rating of the voltage and current limits of the power converter switches $V_{c,max}$ and $I_{c,max}$. For each working point, the boundary of reactive power deviation available for the control action must be contained within the capability curve defined by:

$$\begin{aligned} q_s^c[t_k] &= \sqrt{\left(v_s^2[t_k] I_{c,max}\right)^2 - p_s^2[t_k]} \\ q_s^v[t_k] &= \sqrt{\left(\frac{V_{c,max} v_s[t_k]}{X_c}\right)^2 - p_s^2[t_k]} - \frac{v_s^2[t_k]}{X_c} \\ q_s[t_k] &= \min\left(q_s^c[t_k], q_s^v[t_k]\right). \end{aligned} \tag{A.5}$$

APPENDIX B

Within the simulation framework we make use of *BESS*s as storage devices connected to the test μg feeder by means of *PEI*s, thus using the approach to the reactive/active power support outlined in Section IV and Appendix A. We consider the *BESS* equipped with a battery management system (*BMS*) capable to monitor the battery state of health and to equalize the charging and discharging actions among the batteries composing the *BESS*. We assume the *BMS* communicates the parameters to the microgrid controller in order to allow the computation of the optimization procedure.

Being the focus of the paper on power-flow based studies, we adopt a simplified equivalent circuit, consisting in a voltage source v_{oc} and an internal resistance R_{ESS} being functions of the battery state of charge (*s.o.c.*). The *s.o.c.* is computed based on the charging current of the battery system i_{ESS}, as in (B.1) [28], where p_s represents the power drawn/injected to the grid with sign. The parameters $v_{oc}(s.o.c.)$ and $R_{ESS}(s.o.c.)$ are modeled as characteristic curves derived from battery datasheets available for the proposed commercial solution [24].

$$i_{ESS}[t_k] = -\frac{v_{oc}[t_k]}{2R_{ESS}} + \sqrt{\left(\frac{v_{oc}[t_k]}{2R_{ESS}}\right)^2 + \frac{p_s[t_k]}{R_{ESS}}}. \tag{B.1}$$

Considering the *s.o.c.* as a function of the battery current and taken into account the conversion efficiencies during the charging (η_c) and discharging (η_d) phases through the *PEI*, we compute the *s.o.c.* equation as:

$$SoC[t_k] = SoC[t_{k-1}] \pm \eta_{c,d} \frac{\Delta v_c[t_k] i_{ESS}[t_k] \Delta t_k}{C_{ESS}}, \tag{B.2}$$

where $v_c[t_k]$ is the converter voltage outlined in Fig. A.1 and $\eta_{c,d}$ is representative of η_c during the charging phase and η_d during the discharging phase, while C_{ESS} represents the *BESS* capacity [Wh]. Thus, we introduce in the simulation framework the following constraint related to the *BESS* system *s.o.c.*:

$$s.o.c.^m \leq s.o.c.[t_k] \leq s.o.c.^M. \tag{B.3}$$

Even if the simulation framework is based on a snapshot analysis, we also introduce the *BESS* ramping requirements to assure the adaptation of the state changes:

$$-\Delta s.o.c. \leq \Delta s.o.c.[t_k] \leq \Delta s.o.c., \tag{B.4}$$

where $\Delta s.o.c.$ represents the ramping limit of the *BESS*. We also make use of constraints represented in (17) to (19). During the *g.c.m.*, the *BESS* charging is based on a trade-off between technical and economical constraints. During the *i.o.m.* a further constraint related to the availability of excess power within the network is taken into account: if, for such a reason, the *BESS* is fully discharged and a load curtailment is active because of a shortness of energy within the μg, the storage system is turned off waiting for the energy shortfall period ending.

REFERENCES

[1] T. L. Vandoorn, B. Meersman, J. D. M. De Kooning, and L. Vandevelde, "Transition from islanded to grid-connected mode of microgrids with voltage-based droop control," *IEEE Trans. Power Syst.*, vol. 28, no. 3, pp. 2545–2553, Aug. 2013.

[2] C. Marnay, N. Zhou, M. Qu, and J. Romankiewicz, "International microgrid assessment: Governance, incentives, and experience (IMAGINE)," [Online]. Available: http://der.lbl.gov/sites/der.lbl.gov/files/LBNL-5914E.pdf, pp. 1–103, 2012

[3] A. H. Etemadi, E. J. Davison, and R. Iravani, "A decentralized robust control strategy for multi-DER microgrids-part I: Fundamental concepts," *IEEE Trans. Power Del.*, vol. 27, no. 4, pp. 1843–1853, Oct. 2012.

[4] A. Casavola, G. Franz, D. Menniti, and N. Sorrentino, "Voltage regulation in distribution networks in the presence of distributed generation: A voltage set-point reconfiguration approach," *Elect. Power Syst. Res.*, vol. 81, pp. 25–34, 2011.

[5] M. S. P. Carvalho, P. F. Correia, and L. A. F. M. Ferreira, "Distributed reactive power generation control for voltage rise mitigation in distribution networks," *IEEE Trans. Power Syst.*, vol. 23, no. 2, pp. 766–772, May 2008.

[6] A. Keane, L. F. Ochoa, E. Vittal, C. J. Dent, and G. P. Harrison, "Enhanced utilization of voltage control resources with distributed generation," *IEEE Trans. Power Syst.*, vol. 26, no. 1, pp. 252–260, Feb. 2011.

[7] H. Li, F. Li, Y. Xu, D. T. Rizy, and S. Adhikari, "Autonomous and adaptive voltage control using multiple distributed energy resources," *IEEE Trans. Power Syst.*, vol. 28, no. 2, pp. 718–730, May 2013.

[8] Y. P. Agalgaonkar, B. C. Pal, and R. A. Jabr, "Distribution voltage control considering the impact of PV generation on tap changers and autonomous regulators," *IEEE Trans. Power Syst.*, vol. 29, no. 1, pp. 182–192, Jan. 2014.

[9] I. Dzafic, R. A. Jabr, E. Halilovic, and B. C. Pal, "A sensitivity approach to model local voltage controllers in distribution networks," *IEEE Trans. Power Syst.*, vol. 29, no. 3, pp. 1419–1428, May 2014.

[10] P. Jahangiri and D. C. Aliprantis, "Distributed Volt/VAr control by PV inverters," *IEEE Trans. Power Syst.*, vol. 28, no. 3, pp. 3429–3439, Aug. 2013.

[11] T. Sansawatt, L. F. Ochoa, and G. P. Harrison, "Smart decentralized control of DG for voltage and thermal constraint management," *IEEE Trans. Power Syst.*, vol. 27, no. 3, pp. 1637–1645, Aug. 2012.

[12] F. Olivier, P. Aristidou, D. Ernst, and T. Van Custem, "Active management of low-voltage networks for mitigating overvoltage due to photovoltaic units," *IEEE Trans. Smart Grid*, accepted for publication.

[13] M. J. E. Alam, K. M. Muttaqi, and D. Sutanto, "Mitigation of rooftop solar PV impacts and evening peak support by managing available capacity of distributed energy storage systems," *IEEE Trans. Power Syst.*, vol. 28, no. 4, pp. 3874–3884, Nov. 2013.

[14] V. Calderaro, G. Conio, V. Galdi, G. Massa, and A. Piccolo, "Optimal decentralized voltage control for distribution systems with inverter based distributed generators," *IEEE Trans. Power Syst.*, vol. 29, no. 1, pp. 230–241, Jan. 2014.

[15] S. S. Khorramabadi and A. Bakhshai, "Intelligent control of grid-connected microgrids: An adaptive critic-based approach," *IEEE J. Emerg. Select. Topics Power Electron.*, vol. 3, no. 2, pp. 493–504, 2015.

[16] Y.-S. Kim, E.-S. Kim, and S.-I. Moon, "Frequency and voltage control strategy of standalone microgrids with high penetration of intermittent renewable generation systems," *IEEE Trans. Power Syst.*, accepted for publication.

[17] M. Falahi, K. Butler-Purry, and M. Ehsani, "Dynamic reactive power control of islanded microgrids," *IEEE Trans. Power Syst.*, vol. 28, no. 4, pp. 3649–3657, Nov. 2013.

[18] T. L. Vandoorn, B. Renders, L. Degroote, B. Meersman, and L. Vandevelde, "Active load control in islanded microgrids based on the grid voltage," *IEEE Trans. Smart Grid*, vol. 2, no. 1, pp. 139–151, Mar. 2011.

[19] R. A. Walling, R. Saint, R. C. Dugan, J. Burke, and L. A. Kojovic, "Summary of distributed resources impact on power delivery systems," *IEEE Trans. Power Del.*, vol. 23, no. 3, pp. 1636–1644, Jul. 2008.

[20] Y. Degeilh, J. Descloux, and G. Gross, "Simulation of energy storage in a system with integrated wind resources," in *Proc. 17th Power System Comp. Conf.*, 2011, pp. 1–7.

[21] H. Bevrani and S. Shokoohi, "An intelligent droop control for simultaneous voltage and frequency regulation in islanded microgrids," *IEEE Trans. Smart Grid*, vol. 4, no. 3, pp. 1505–1513, Sep. 2013.

[22] M. Farivar, R. Neal, C. Clarke, and S. Low, "Optimal inverter VAr control in distribution systems with high PV penetration," in *Proc. IEEE Power and Energy Soc. General Meeting*, San Diego, CA, USA, 2012, pp. 1–7.

[23] Capstone Turbine Corporation, "Capstone C1000 Microturbine Systems technical reference," [Online]. Available: http://www.regattasp.com/files/ 410072A-C1000-TR.pdf, pp. 49–54, 85–93, 2009

[24] ABB, "Energy storage modules (ESM) Up to 4 MW," [Online]. Available: http://www05.abb.com/global/scot/scot235.nsf/veritydisplay/f09413974e2 f041cc12579e3004fa562/file/energy-storage-modules-brochure-rev-e.pdf, pp. 1–19, 2012

[25] Elexon, Profiling Samples and Candidate Selection [Online]. Available: http://www.elexon.co.uk/reference/technical-operations/profiling/, pp. 1–16, 2013

[26] A. B. Almeida, E. V. De Lorenci, R. C. Leme, A. C. Zambroni de Souza, B. I. Lima Lopes, and K. Lo, "Probabilistic voltage assessment considering renewable sources with the help of the PV and QV curves," *IET Renew. Power Gener.*, vol. 7, no. 5, pp. 521–530, 2013.

[27] B. A. Robbins, C. N. Hadjicostis, and A. D. Domnguez-Garca, "A two-stage distributed architecture for voltage control in power distribution systems," *IEEE Trans. Power Syst.*, vol. 28, no. 2, pp. 1470–1482, May 2013.

[28] J. von Appen, T. Stetz, M. Braun, and A. Schmiegel, "Local voltage control strategies for PV storage systems in distribution networks," *IEEE Trans. Smart Grid*, vol. 5, no. 2, pp. 1002–1009, Mar. 2014.

Giovanni Massa (M'12) received the M.Sc. degree in Electronic Engineering in 2009 and the Ph.D. degree in Information Engineering in 2013, both from the University of Salerno, Italy. His main research interests focus on smart grid development issues, including integration of distributed energy resources into distribution networks and microgrids, soft computing methodologies for power system applications, energy saving in electric transportation, and intelligent transportation systems.

George Gross (F'88) is Professor of Electrical and Computer Engineering and Professor, Institute of Government and Public Affairs, at the University of Illinois at Urbana-Champaign. His current research and teaching activities are in the areas of power system analysis, planning, economics and operations and utility regulatory policy and industry restructuring. In the 1999–2000 academic year, he was a Visiting Professor at a number of Italian institutions including University of Pavia, Politecnico di Milano and Politecnico di Torino. His undergraduate work was completed at McGill University, and he earned his graduate degrees from the University of California, Berkeley. He was previously employed by Pacific Gas and Electric Company in various technical, policy and management positions. Dr. Gross won the Franz Edelman Management Science Achievement Award in 1985 and is the recipient of several prize paper awards. He has consulted widely to organizations in North and South America, Europe and Asia.

Vincenzo Galdi (M'98) received the M.Sc. degree in Electronic Engineering from the University of Salerno, Fisciano, Italy, in 1994, and the Ph.D. degree in Electrical Engineering from the University of Napoli, Napoli, Italy, in 1999. Since 2003, he has been an Associate Professor at the University of Salerno, now in the Department of Industrial Engineering. His current research interests include application of ICT to power systems, to power management and energy efficiency in transportation systems, smartgrids and ITS.

Antonio Piccolo (M'06) received the M.Sc. degree in Electrical Engineering in 1974 from the University of Napoli. Since 1990 he is Full Professor at University of Salerno, Italy, now as founding member of Department of Industrial Engineering. His main fields of interest are the application of ICT to electric energy infrastructures and transportation systems. He served as reviewer and session chairman for many international conferences. Prof. Piccolo is a Chartered Engineer and has authored more than 130 papers mainly in international journals and conferences in the field of power systems.